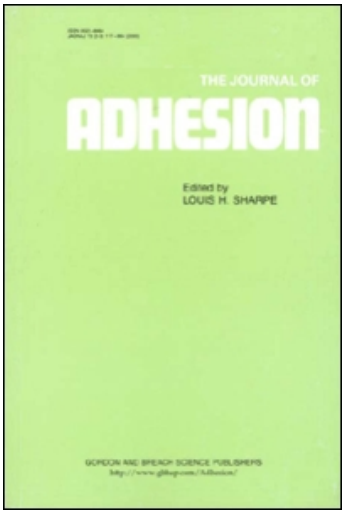

The Journal of Adhesion
Publication details, including instructions for authors and subscription information:
http://www.informaworld.com/smpp/title~content=t713453635

Adhesion of a Fibrillar Interface on Wet and Rough Surfaces

Shilpi Vajpayee[a]; Anand Jagota[a]; C. -Y. Hui[b]
[a] Department of Chemical Engineering and Bioengineering Program, Lehigh University, Bethlehem, USA [b] Department of Theoretical and Applied Mechanics, Cornell University, Ithaca, NY, USA

Online publication date: 05 February 2010

To cite this Article Vajpayee, Shilpi , Jagota, Anand and Hui, C. -Y.(2010) 'Adhesion of a Fibrillar Interface on Wet and Rough Surfaces', The Journal of Adhesion, 86: 1, 39 — 61
To link to this Article: DOI: 10.1080/00218460903417834
URL: http://dx.doi.org/10.1080/00218460903417834

The Journal of Adhesion, 86:39–61, 2010

ISSN: 0021-8464 print/1545-5823 online
DOI: 10.1080/00218460903417834

Taylor & Francis
Taylor & Francis Group

Adhesion of a Fibrillar Interface on Wet and Rough Surfaces

Shilpi Vajpayee[1], Anand Jagota[1], and C.-Y. Hui[2]
[1]Department of Chemical Engineering and Bioengineering Program, Lehigh University, Bethlehem, USA
[2]Department of Theoretical and Applied Mechanics, Cornell University, Ithaca, NY, USA

We have studied the adhesion of a biomimetic fibrillar interface terminated by a thin film in aqueous medium and against dry rough surfaces to simulate more realistic environmental conditions. We consistently observed enhancement of adhesion under water (compared with measurements in air) against hydrophobic surfaces for all samples. In most cases, adhesion could be represented by a multiplicative coupling between crack-trapping due to the architecture and the intrinsic work of adhesion. With increasing inter-fibrillar separation, adhesion first increases and then usually decreases. The decrease in adhesion for large inter-fibrillar separations can be explained by a transition in the controlling mechanism for interfacial separation from crack-trapping to stress-controlled nucleation of interfacial voids. Against rough surfaces, as roughness was increased, all samples showed a reduction in adhesion but fibrillar surfaces retained significant adhesion even when flat surfaces had almost none.

Keywords: Adhesion; Crack-trapping; Fibrillar; Roughness; Under water; Void nucleation

1. INTRODUCTION

Many natural systems, such as the feet of geckos and many insects, display extraordinarily strong non-specific adhesion to a variety of

Received 15 March 2009; in final form 10 August 2009.
One of a Collection of papers honoring J. Herbert Waite, the recipient in February 2009 of *The Adhesion Society Award for Excellence in Adhesion Science, Sponsered by 3M*.
Address correspondence to Anand Jagota, Department of Chemical Engineering, 111 Research Drive, D311 Iacocca Hall, Lehigh University, Bethlehem, PA 18017, USA. E-mail: anj6@lehigh.edu

surfaces [1–8]. A common structural motif is a fibrillar architecture terminated by thin compliant elements [9–15]. This has inspired many researchers to fabricate biomimetic fibrillar structures, many of which exhibit significant enhancement in adhesion and friction [9,10,13, 15–20]. We have developed a design that consists of an array of fibrils emanating from a thick base and terminated by a thin roof—a continuous thin plate that connects all the fibrils. Structures with this design fabricated using poly(dimethyl siloxane) (PDMS) have significantly enhanced adhesion and static friction (in air) compared with a flat control made of the same material [10,19,21]. Most previous studies of the adhesion of fibrillar structures have been conducted under ambient conditions and against smooth surfaces. To explore more fully their potential for use in applications, it is necessary to examine the behavior of these structures under more realistic environmental conditions. In this work we present preliminary results on the adhesion of film-terminated fibrillar structures under water and against rough surfaces.

Adhesion studies of hydrophobic surfaces under water generally report works of adhesion exceeding significantly those observed between the same surfaces in air; separation is often accompanied by cavitation [22–26]. These interactions are longer in range than the hydration repulsion and are 10 to 100 times stronger than van der Waals forces. Yushchenko *et al.* [27] have shown theoretically that a stable cavity can form between two hydrophobic surfaces if the contact angle is greater than 90° and this vapor bridge can contribute significantly to the attraction between surfaces. Christensen and Claesson [23] observed spontaneous cavitation when fluorocarbon surfaces were brought into contact in deaerated water but only after some separation. The long-range attractive forces were attributed to metastability of water films between two hydrophobic surfaces. Chaudhury and Whitesides [22] studied adhesion of smooth PDMS surfaces in water and noticed the formation of a ring of vapor at the contact line when experiments were done in pure water. They found that this phenomenon could be eliminated by degassing the water, and argued that water is eliminated from the contact region. They showed that adhesion in water is approximately twice the surface tension of the water/solid interface (about $75\,mJ/m^2$), considerably larger than the value of $45\,mJ/m^2$ measured in air. Singh *et al.* [25]. showed that for rough superhydrophobic surfaces submerged in deaerated water, cavitation occurs over very large distances (ranging from 0.8 to 3.5 microns). They argued that capillary-like fluctuations of vapor films grow, extending from the superhydrophobic surfaces, leading to the sudden formation and growth of a vapor bridge. They reported that

after the two surfaces have been separated, a cavity bubble remains on the surfaces and vanishes after some time.

Most of the works cited above are based on adhesion against unstructured hydrophobic surfaces under water. Since fibrillar structures have already shown enhanced adhesion in dry conditions, it is interesting to ask whether this effect is maintained under water. Lee *et al.* [28]. measured the underwater adhesion of their nano-scale fibrillar samples and found that it is improved considerably by coating their samples with a thin film of poly(dopamine methacrylamide-co-methoxyethyl acrylate) [p(DMA-co-MEA)]. Their adhesion enhancement mechanism relies on specific chemical interactions, whereas other fibrillar structures (including the film-terminated version we have developed) are based on generic adhesion interactions amplified by design of the structure. Varenberg and Gorb [29] showed some improvement in adhesion in the presence of water for a "mushroom"-shaped fibrillar microstrucutre.

A vast literature is available on the effect of roughness on adhesion between unstructured surfaces. Fuller and Tabor [30], followed by others, observed a monotonic decrease in adhesion with increasing surface roughness. This was understood by developing several theoretical models. Fuller and Tabor [30] modeled roughness as asperities, each with the same radius of curvature, having heights that follow a Gaussian distribution. They applied the contact theory of Johnson, Kendall, and Roberts [31] (JKR) to individual asperities to calculate the net contact force, and derived an adhesion parameter that represents the competition between compressive forces exerted by higher asperities trying to pry the surfaces apart and adhesive forces between lower asperities trying to hold the surfaces together. Briggs and Bricoe [32] offered an alternative explanation by noting that the JKR contact theory, when applied on single asperities, predicts that on separation they carry an excess stored elastic energy, which is lost. Later, Fuller and Roberts [33] showed that their argument is flawed and attributed the increase in work of adhesion to viscoelasticity. Specifically, the stored elastic energy in asperities, which would normally assist in separation, is lost *via* stress relaxation. Once the surfaces conform to make good contact with no stored elastic energy due to deformation, the real contact area in the presence of roughness is higher and, hence, work of adhesion is higher. Also, isolated contact points at final stages of pull-off lead to irreversible loss of elastic energy built up during peeling, increasing the energy required to separate the surfaces. Similarly, Kim and Russell [34] studied adhesion of PDMS to rough aluminium surfaces and observed an initial increase in adhesion with increasing roughness. Persson and Tosatti [35] and Persson [36]

modeled the effect of roughness by defining an effective work of adhesion. Compared with the true work of adhesion, it has a positive contribution from an increase in real contact area and a negative contribution due to release of elastic energy stored in asperities. These two competing effects offered one explanation for an enhancement in adhesion with increasing roughness at very low roughness. More recently, Guduru [37] has investigated the effect of surface waviness on adhesion. He showed that if there is a complete contact initially, then surface separation is alternately stable and unstable. The loss of energy during unstable separation leads to an increase in effective work of adhesion. His theory is confirmed by experiments which showed that unstable separation can lead to a very large increase in adhesion in perfectly elastic solids [38].

All the above-mentioned studies have been conducted with rough surfaces against a smooth surface. Theoretical studies [39,40] have shown how increased compliance can compensate for the deleterious effects of surface roughness. Whether fibrillar structures indeed do maintain their advantage against rough surfaces is, therefore, an interesting question.

The remainder of the paper is organized as follows. Section 2 describes experimental methods. In section 3.1, we report on the adhesion of film-terminated fibrillar samples under water. Adhesion is measured using an indentation experiment. Using the same method, in Section 3.2, we present data on the effect of surface roughness on adhesion of these structures. We conclude with a summary in Section 4.

2. EXPERIMENTAL METHODS

2.1. Indentation Tests

Indentation experiments were conducted using a custom-built apparatus that has been described previously [19]. Briefly, the sample is placed on the stage of an inverted microscope and a glass sphere is lowered onto the sample using a motorized vertical stage. The sphere is brought in contact and further indented into the sample up to a prescribed distance and then retracted until contact between the sample and sphere is lost. The rate of motion of the spherical indenter is kept constant at $1\,\mu m/s$. Force during the test is measured using an in-line load cell and the displacement of the indenter is obtained from the motion of the motorized vertical stage. The contact area between the sample and indenter is monitored during the test through the inverted microscope and captured by a commercial digital camera.

The displacement of the indenter is corrected for machine compliance by separately measuring the latter by performing an indentation experiment on a stiff plate. The fibrillar samples and a flat control sample were indented with a glass sphere coated by a hydrophobic self-assembled monolayer (SAM), a PDMS-coated glass sphere, and a hydrophilic glass sphere. The tests are done in air as well as under de-ionized water. The samples are indented sufficiently deeply so that the response during retraction is independent of preload [41].

2.2. Adhesion Tests Against Rough Surfaces

Indentation tests were performed on fibrillar samples and a flat control sample using spherical indenters with varying surface roughness. The method for preparation of these indenters with a rough surface is discussed in Section 2.7.

2.3. Sample Fabrication

Film-terminated fibrillar samples were fabricated as described previously [10]. Briefly, a fibrillar surface was obtained by molding uncured PDMS (Sylgard® 184; Dow Corning, Midland, MI, USA) base and cure mixture (10:1 weight ratio) in negative silicon masters which were patterned by photolithography and deep reactive ion etch techniques. The PDMS base and cure mixture were first degassed in house vacuum for 30 minutes and then poured in the silicon masters where it was allowed to crosslink at 80°C for 2 hours. The thin film at the top of the fibrils was obtained by spin-coating uncured PDMS base and cure mixture (10:1 ratio) on a silanized silicon wafer, placing the fibrils in contact with it, followed by curing at 80°C for an hour. Samples studied in this work consist of fibrils with a square cross section 10 μm on a side and height of 53 or 30 μm, arranged in an hexagonal or a square pattern, respectively, on a 0.635 mm thick base of PDMS. These fibrils are topped with a thin film of PDMS which is approximately 4 μm in thickness. Three different samples with an hexagonal arrangement of fibrils and nearest neighbor inter-fibrillar spacings of 38, 62, and 87 μm were used. Four different samples with a square arrangement of fibrils and nearest neighbor inter-fibrillar spacings of 35, 50, 65, and 80 μm were used.

2.4. Self-Assembled Monolayer Deposition

A hydrophobic self-assembled monolayer (SAM) of n-hexadecyltrichlorosilane was assembled on a glass sphere approximately

6.26 mm in diameter to reduce its surface energy. The glass sphere was first cleaned in a solution of 70% H_2SO_4, 15% H_2O_2, and 15% H_2O for 0.5 hours and then cleaned in O_2 plasma for 1 minute. After plasma treatment it was treated with silane vapors for an hour at low pressure. Details of this procedure have been given previously [10].

2.5. Preparation of PDMS-Coated Glass Sphere

A glass sphere approximately 6.25 mm in diameter was coated with PDMS. This was done by cleaning the glass sphere in a solution of 70% H_2SO_4, 15% H_2O_2, and 15% H_2O for 0.5 hours and then dipping it in the uncured PDMS base and cure (10:1 weight ratio) mixture which had been degassed in house vacuum for 30 minutes. The glass sphere was then allowed to stand vertically for 5 minutes at room temperature after which it was placed in an oven at 80°C for 2 hours to cure the PDMS. The thickness of the PDMS layer was measured using an optical microscope and was found to be around 50–60 μm. (For comparison, the contact diameter at pull-off is at least 400 μm.) The finite thickness of PDMS makes the indenter slightly compliant which means that, strictly, one cannot compare the pull-off force measured using this and the SAM-coated indenter. However, as described later in Section 3.1, we extract the work of adhesion from these measurements in a manner that does not require us to know the thickness of PDMS layer on the indenter.

2.6. Preparation of Hydrophilic Glass Sphere

A glass sphere approximately 6.25 mm in diameter is cleaned in a solution of 70% sulfuric acid, 15% hydrogen peroxide, and 15% water for 0.5 hours and then cleaned in O_2 plasma for 1 minute. The surface of the sphere is exposed to de-ionized water for some time and brought in contact with PDMS several times to condition it before conducting the indentation experiments.

2.7. Preparation of Rough Surface

Glass spheres approximately 4 mm in radius were used as the contacting surface for the adhesion tests. To vary the surface roughness, these glass spheres were painted with different commercial paints (Olympic Premium, Interior latex, and PPG Architectural Finishes, Pittsburgh, PA, USA) called “gloss,” “semi-gloss,” “satin,” “eggshell,” and “flat” in order of increasing roughness. The paint was applied by dipping the spheres in it and then holding them vertically with

the contacting surface pointing up to let the paint flow to form a macroscopically uniform coating before it dried.

2.8. Contact Angle Measurement

To determine the hydrophobicity of the samples and indenters, the contact angle of water on these surfaces was measured. The surface to be tested was placed on a horizontal stage and a drop of water was released on it and removed using a micro-pipette. Images of the water drop on the surface were recorded through a long-range microscope and used to measure the advancing and receding contact angles.

3. EXPERIMENTAL RESULTS AND DISCUSSION

3.1. Adhesion Under Water

Figures 1a–d show typical force-displacement data measured during indentation (using SAM-coated, PDMS-coated, and hydrophilic glass spheres) in air and under water of a flat control sample and fibrillar samples. We observed an increase in pull-off force under water over that measured in air for both the fibrillar and the flat control samples when hydrophobic SAM-coated and PDMS-coated indenters were used. When the fibrillar and flat control samples were indented with the hydrophilic indenter, the pull-off force was lower when the test was done under water as compared with that measured when the test was conducted in air. These data were taken after repeated indentations and after the sample and the indenter both had been immersed in water for at least 10 minutes. On immersion of a dry hydrophobic indenter into water, we often observed cavitation in the form of a vapor ring around the contact. On indenter retraction the ring would shrink with the contact and coalesce into a bubble forming an enclosed vapor bridge between the sample and the indenter surfaces. Eventually, the bridge severed, leaving a bubble each on the sample and indenter surfaces; these were observed to vanish within a few minutes. After repeated indentations keeping the indenter and sample immersed (over a period of about 10 minutes), cavitation was no longer observed with either the SAM-coated or the PDMS-coated glass spheres. The advancing and receding contact angles on the SAM-coated sphere were 110° and 105°, respectively. The advancing contact angles for flat and fibrillar samples (with inter-fibrillar spacing of 38, 62, and 87 μm) were found to be approximately 117°, 126°, 135°, and 133°, respectively. Receding contact angles were measured to be approximately 70°, 36°, 35°, and 23° in the same order.

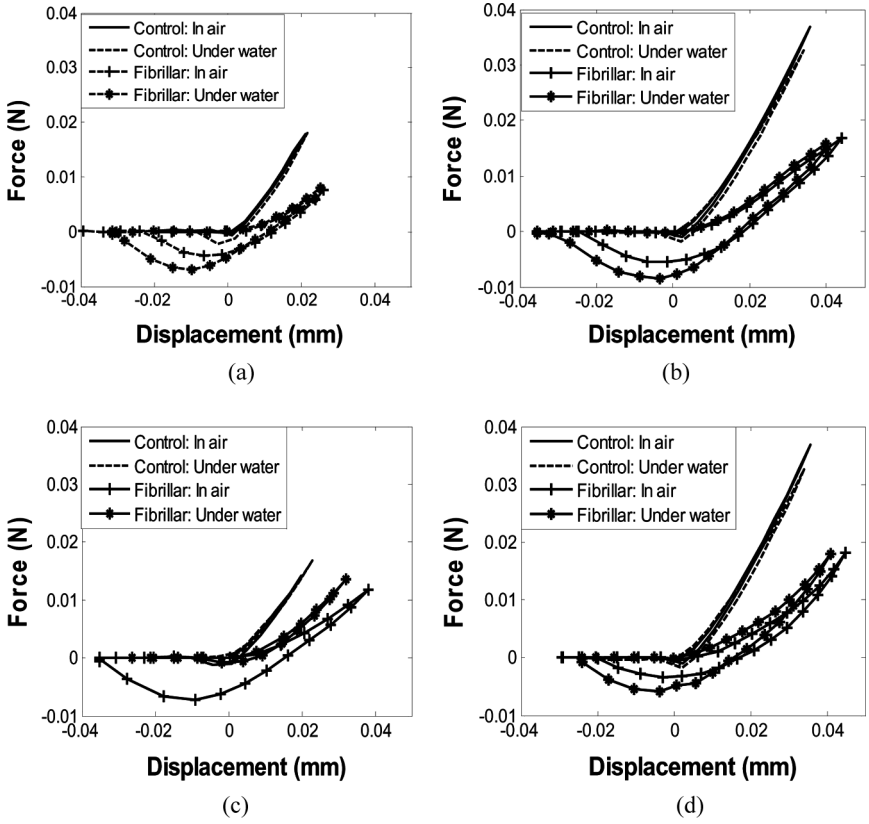

FIGURE 1 Force-displacement plots for indentation tests on a fibrillar sample (fibril height of 53 μm; inter-fibrillar spacing of 87 μm with fibrils arranged in hexagonal pattern) and a flat control sample by a (a) SAM-coated glass sphere, (b) PDMS-coated glass sphere, (c) Hydrophilic glass sphere under water and in air, and (d) Force-displacement plots for normal indentation tests on a fibrillar sample (fibril height of approximately 30 μm and inter-fibrillar spacing of 80 μm with fibrils arranged in square pattern) and a flat control sample by a PDMS-coated glass sphere under water and in air.

Our contact angle measurement for flat PDMS matches closely with that reported by He *et al.* [41]. for the same type of PDMS (Sylgard® 184 Silicone Elastomer Kit, Dow Corning, Midland, MI, USA). The increase in hysteresis on the fibrillar samples is noteworthy, possibly by a contact line trapping mechanism analogous to the crack-trapping that enhances adhesion in this system [19,43]. The low value of the receding contact angle probably accounts for the fact that we did not observe spontaneous cavitation.

Figures 2a–d plots pull-off force for different samples as a function of inter-fibrillar spacing; zero spacing represents flat control. The increase in adhesion under water seen in Figs. 1(a, b, d) is reproduced in all samples. However, a decrease in adhesion is seen in Fig. 1(c) when samples are tested against a hydrophilic indenter under water. The data in Figs. 2(a, b, d) show qualitatively that, in most cases, the pull-off force increases by a similar factor independent of the inter-fibrillar spacing, consistent with a multiplicative coupling between crack-trapping and intrinsic work of adhesion [43]. For a SAM-coated indenter, the pull-off force is found to be highest in the sample with intermediate inter-fibrillar spacing, and this trend is

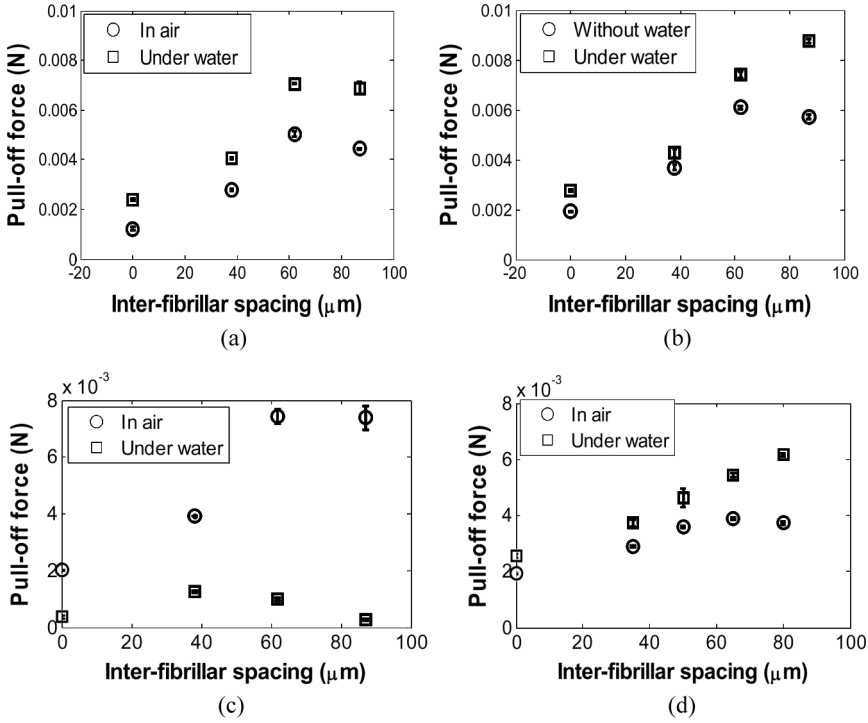

FIGURE 2 Pull-off force as a function of inter-fibrillar spacing obtained from indentation tests on fibrillar samples (with hexagonal arrangement of fibrils) in air and under water with (a) SAM-coated glass sphere, (b) PDMS-coated glass sphere, (c) hydrophilic glass sphere, and (d) Pull-off force as a function of inter-fibrillar spacing obtained from indentation tests on samples (with square arrangement of fibrils) in air and under water with PDMS-coated glass sphere.

replicated under water. However, for indentation on samples with an hexagonal as well as a square arrangement of fibrils with the PDMS-coated glass sphere, samples with the largest inter-fibrillar spacing were found to have the highest pull-off force under water. A different trend was observed when samples were indented by a hydrophilic sphere under water, as shown in Fig. 2(c). In that case, pull-off force was highest for the sample with the smallest inter-fibrillar spacing and was lowest for the sample with the largest inter-fibrillar spacing (close to that of the flat control sample). In the case of the sample with largest inter-fibrillar spacing, considerable buckling of fibrils was observed under water *even before* the hydrophilic sphere came into contact with the sample, and it continued during indentation. That is, the force exerted by the indenter to squeeze out the water between the indenter and the sample surface before contact was sufficient to buckle the fibrils.

A two-dimensional model for crack-trapping predicts that, as long as this mechanism controls it, adhesion should increase monotonically with increasing inter-fibrillar spacing [19,44]. However, Fig. 2 shows the appearance of a maximum pull-off load in tests with the SAM-coated sphere at an intermediate fibril spacing, consistent with a wider range of data for adhesion in air, presented elsewhere [19]. This phenomenon was also observed in friction experiments [21] which strongly suggested that static friction is essentially governed by the same crack-trapping mechanism. Indeed, static friction was found to increase with inter-fibrillar spacing and achieved a maximum when the separation mechanism shifted to fibril fracture. With further increase in fibril spacing static friction decreases, primarily because the failure mechanism is now limited by the failure strength of fibrils.

We ask whether an analogous competition between two mechanisms for interfacial separation operates during normal indentation. The first is the crack-trapping mechanism, under which adhesion should increase with increasing spacing between fibrils. In this mechanism, interfacial separation is governed by the condition that the energy release rate at the crack tip (the contact line in an indentation test) be sufficient for it to propagate. Enhancement in adhesion is achieved by modulating the energy release rate which varies depending on the position of the crack tip. As the inter-fibrillar spacing increases, the minimum energy release rate which occurs just before the crack reaches a fibril becomes vanishingly small, requiring higher remote loading to propagate the interface crack. On the other hand, increase in remote loading also increases the tensile stress under fibrils ahead of the crack tip. Eventually, the increase in stress on a fibril is limited by the nucleation of cavities in the contact patch

ahead of the retracting contact line (crack tip), presumably governed by a characteristic cavitation stress as in the Cook-Gordon mechanism [45]. When failure is governed by cavitation (or void nucleation), further increase in spacing between fibrils is detrimental since the density of load-bearing fibers will decrease. Therefore, competition between these two mechanisms (interfacial crack growth *versus* failure by nucleation of cavities) is expected to result in an optimal value of fibril spacing for interfacial toughness. A simple model to understand how adhesion is affected by inter-fibrillar spacing is presented below.

When a rigid sphere of radius R is indented into a macroscopically flat sample, the surface displacement δ of the sample varies with the distance, x, from the center of contact as:

$$\delta = \Delta - \frac{x^2}{2R}, \tag{1}$$

where Δ is the indentation depth of sphere (*i.e.*, indentation depth at the centre) and R is the radius of the sphere. Equation (1) assumes that the contact is small so that the sphere can be represented in the contact region as a paraboloid. Let σ_c be the absolute value of cavitation stress. As in Long *et al.* [46], the fibril interface is treated as an elastic spring foundation, with stiffness $k = EA/L$, where A is the cross-sectional area of the fibril, E is the elastic modulus of the material, and L is the fiber length. Ignoring the elasticity of the backing layer, the displacement of the surface is due entirely to the deformation of the spring foundation (the fibrillar interface). The tensile stress at a fibril subjected to an extension of $-\delta$ is $-k\delta/A$ (Note: positive force means compression). Once the absolute value of tensile stress on a fibril reaches σ_c, nucleation of cavities at the fibrils limits further increase in stress at the fibrils for the same contact area. This condition can be used to deduce the contact size, that is:

$$\begin{aligned} & -k\delta/A \le \sigma_c \\ & \Rightarrow -k\left(\Delta - \frac{x^2}{2R}\right) \le \sigma_c A \\ & \Rightarrow x \le \sqrt{2R\left(\Delta + \frac{\sigma_c A}{k}\right)} \\ & \therefore a = \sqrt{2R\left(\Delta + \frac{\sigma_c A}{k}\right)}, \end{aligned} \tag{2}$$

where a is the contact radius for a given indenter displacement, Δ. Net force on the indenter during the indentation process is given by

$$F = \int_0^a \sigma_{yy}(2\pi x)dx = \int_0^a k\delta\Sigma(2\pi x)dx = \pi k\Sigma\left(\Delta a^2 - \frac{a^4}{4R}\right). \quad (3)$$

Eliminating a from Eq. (3) by using Eq. (2) yields:

$$F = \pi k\Sigma R\left[\Delta^2 - \frac{\sigma_c^2 A^2}{k^2}\right], \quad (4)$$

where Σ is the number of fibrils per unit area. For an hexagonal arrangement of fibrils, its dependence on the inter-fibrillar spacing, w, is $\Sigma = \frac{2}{\sqrt{3}w^2}$, while for a square arrangement of fibrils, $\Sigma = \frac{1}{w^2}$. The pull-off force, *i.e.*, the maximum tensile force on the indenter is achieved at $\Delta = 0$, that is,

$$F_{\text{pull-off}} = -\pi\Sigma R\frac{\sigma_c^2 AL}{E}. \quad (5)$$

Because the number of fibrils per unit area is inversely proportional to the square of inter-fibrillar spacing, this model predicts that pull-off force decreases inversely with w^2 when interfacial separation is controlled by void nucleation under the fibrils. In the other limit, where stress concentration is important, pull-off is controlled by the crack-trapping mechanism; Shen *et al.* [44] predicted that the work of adhesion is proportional to the fourth power of inter-fibrillar spacing. The following derivation, which is similar to one by Schargott *et al.* [47], establishes that if the elasticity of the backing layer can be neglected, then the pull-off force is directly proportional to the work of adhesion.

The elastic strain energy stored in the fibrils when they are indented by a rigid sphere is:

$$U_e = \int_0^a \frac{1}{2}k\delta^2\Sigma(2\pi x)dx = \frac{\pi k\Sigma}{2}\left[a^2\Delta^2 + \frac{a^6}{12R^2} - \frac{\Delta a^4}{2R}\right]. \quad (6)$$

The total energy of the system includes the contribution from adhesive forces along with the elastic strain energy:

$$U_t = U_e - (\pi a^2)W_{ad}. \quad (7)$$

The condition for contact is obtained by equating energy release rate to work needed to propagate the contact line, *i.e.*,

$$\begin{aligned} G &= \frac{dU_t}{da} = 0 \quad \text{for contact} \\ \Rightarrow a^2 &= 2\Delta R \pm \sqrt{\frac{8W_{ad}R^2}{k\Sigma}}. \end{aligned} \tag{8}$$

Normal force can be obtained by eliminating a in Eq. (3) using Eq. (8):

$$\begin{aligned} F &= 2R\pi k\Sigma\left[\frac{\Delta^2}{2} - \frac{W_{ad}}{k\Sigma}\right] \\ \Rightarrow F_{\text{pull-off}} &= -2\pi R W_{ad}. \end{aligned} \tag{9}$$

In Eq. (9), W_{ad} is to be interpreted as the effective work of adhesion for contact line retraction, accounting for adhesion enhancement due to crack-trapping. The crack-trapping model of Shen *et al.* [44] implies that the effective work of adhesion under the crack-trapping mechanism increases with the fourth power of w. Since the effective work of adhesion must be the same as the intrinsic work of adhesion for $w = 0$, we assume that W_{ad} has the form

$$W_{ad} = W_o\left(1 + \alpha w^4\right), \tag{10}$$

where W_o is the work of adhesion of an unstructured flat control sample and α is a constant which depends on material properties and geometry (but is independent of w). In the limit where the spacing is very large, interfacial opening is governed by void nucleation and the contact radius is given by Eq. (2). By matching Eq. (5) with Eq. (9), we can associate an effective work of adhesion with the void nucleation mechanism:

$$\begin{aligned} W_{ad} = \frac{\sigma_c^2 A^2 \Sigma}{2k} &= \frac{\sigma_c^2 A l}{\sqrt{3}E}\left(\frac{1}{w^2}\right) \quad \text{for hexagonal arrangement of fibrils} \\ &= \frac{\sigma_c^2 A l}{2E}\left(\frac{1}{w^2}\right) \quad \text{for square arrangement of fibrils} \\ &= \frac{\beta}{w^2}. \end{aligned} \tag{11}$$

That is, effective work of adhesion associated with void nucleation should also decrease inversely with the square of inter-fibril spacing under the void nucleation condition.

The value of W_o is determined from experiments on control samples and the effective work of adhesion for fibrillar samples is calculated from experimental data (load, displacement, and contact area) using the method presented in Vajpayee *et al.* [48], assuming the work of adhesion during loading to be much smaller than during unloading. Values of the coefficients α and β are chosen to fit Eq. (10) and (11) to the measured works of adhesion (Fig. 3). Figure 3 gives an estimate of optimal separation between the fibrils for highest adhesion, the point of intersection of curves predicted from the two models. We measured the value of W_o against the flat PMDS sample to be $90\,\mathrm{mJ/m^2}$

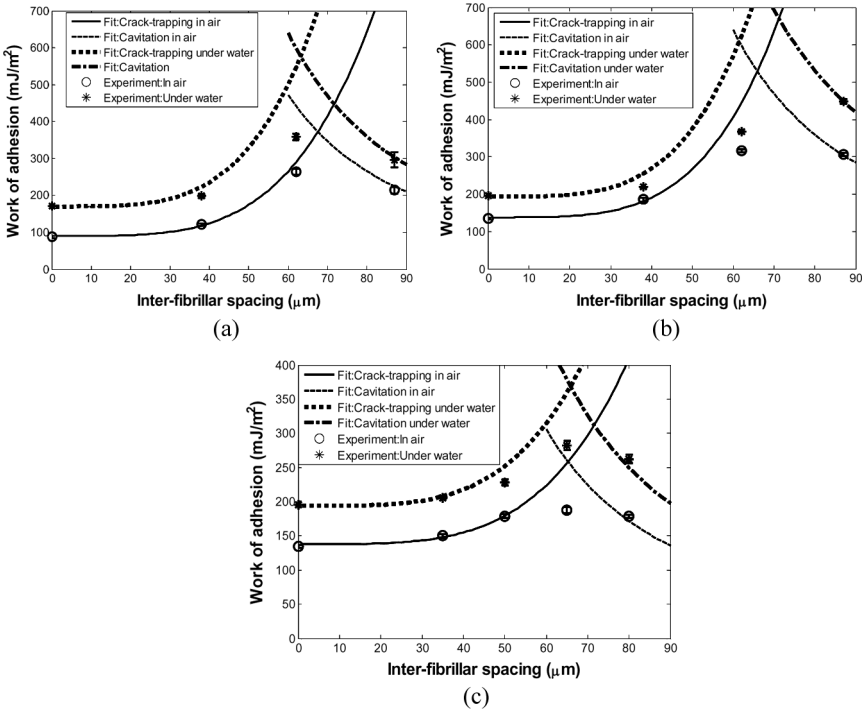

FIGURE 3 Work of adhesion as a function of inter-fibrillar spacing (w) for indentation tests done on fibrillar samples (with fibrils arranged in a hexagonal pattern) with (a) SAM-coated glass sphere, (b) PDMS-coated glass sphere, and (c) Work of adhesion as a function of inter-fibrillar spacing (w) for indentation tests done on fibrillar samples (with fibrils arranged in a square pattern) with PDMS-coated glass sphere. Also shown are the predictions based on crack-trapping and void nucleation modes of interfacial separation. [*Note*: The smallest spacing in this plot ($w = 0$) corresponds to the flat PDMS sample.]

(in air) and $170\,mJ/m^2$ (under water) for the SAM-coated indenter and $138\,mJ/m^2$ (in air) and $194\,mJ/m^2$ (under water) for the PDMS-coated indenter. The value of parameter α was found to be $1.5 \times 10^{17}\,m^{-4}$ for fibrillar samples with fibrils arranged in an hexagonal pattern and $4.8 \times 10^{16}\,m^{-4}$ for fibrillar samples with fibrils arranged in a square pattern, *i.e.,* enhancement. The cavitation stress, σ_c, for fibrillar samples with fibrils arranged in an hexagonal pattern was found to be 1.3 MPa (in air) and 1.5 MPa (under water) for the SAM-coated indenter and 1.5 MPa (in air) and 1.8 MPa (under water) for the PDMS-coated indenter. The computed values of σ_c for contact between fibrillar samples with fibrils arranged in the square pattern for the PDMS-coated sphere were 1.08 MPa (in air) and 1.31 MPa (under water). All these results show that the critical stress for nucleation of voids is higher under water than in air. Since σ_c is highest when samples are indented under water using the PDMS-coated sphere, the transition from crack-trapping to void nucleation is reached at larger inter-fibrillar spacings. It is interesting to note that the values of cavitation stress are similar in magnitude to the elastic modulus of PDMS, as measured in other experiments and consistent with a statistical model for adhesive strength of compliant materials [49].

Figure 4 presents plots of work of adhesion normalized by that of the corresponding control sample, W_o. According to Eq. (10), the normalized work of adhesion should depend only on material properties and architecture and should be independent of the interfacial work of adhesion. This means that, if adhesion is governed by the crack-trapping mechanism, then the normalized work of adhesion for all fibrillar samples with same architecture should fall on one curve. Figure 4 shows that for all fibrillar samples, the normalized work of adhesion under water is systematically lower than in air. This is because, while both the intrinsic work of adhesion, W_o, and cavitation stress, σ_c, are larger under water than in air (for hydrophobic surfaces), the former increases by a considerably greater factor.

Direct evidence of the nucleation of voids at the interface has been obtained from indentation experiments under water. Figure 5 shows the contact micrographs of the SAM-coated indenter and the fibrillar sample during retraction of the sphere. The inner region surrounded by a boundary is the contact area. This undulating boundary of the contact region is the crack front between the sphere and the sample. On contact growth, which precedes the state shown in this figure, as the contact line sweeps around fibrils, it traps small pools of water, which remain and can be seen in these micrographs (highlighted by the dotted ovals). (During experiments in air, the corresponding trapped air bubbles quickly disappear as the air is absorbed by the

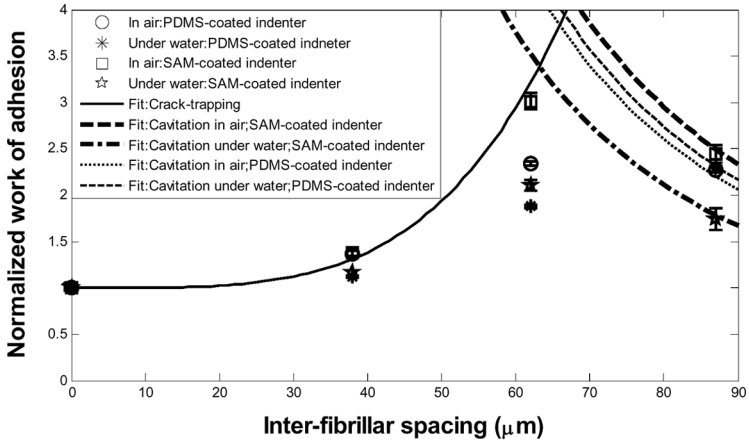

(a)

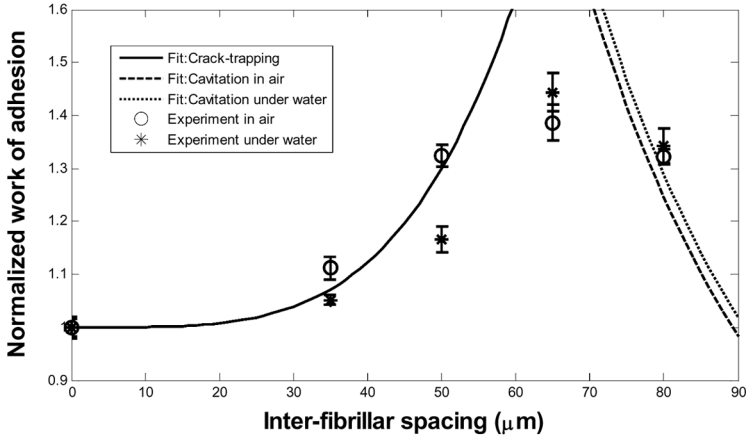

(b)

FIGURE 4 Normalized work of adhesion as a function of inter-fibrillar spacing (w) along with predictions based on crack-trapping and void nucleation modes of interfacial separation normalized with the corresponding W_o for (a) fibrillar samples with fibrils arranged in a hexagonal pattern and (b) fibrillar samples with fibrils arranged in a square pattern. [*Note*: The smallest spacing in this plot ($w = 0$) corresponds to the flat PDMS sample. The work of adhesion for different samples was normalized with the work of adhesion of flat control samples ($w = 0$)].

PDMS.) For the largest spacing samples, we find that many of the pockets of trapped water apparently disappear suddenly as the crack front approaches (Micrographs II–IV). To present this phenomenon

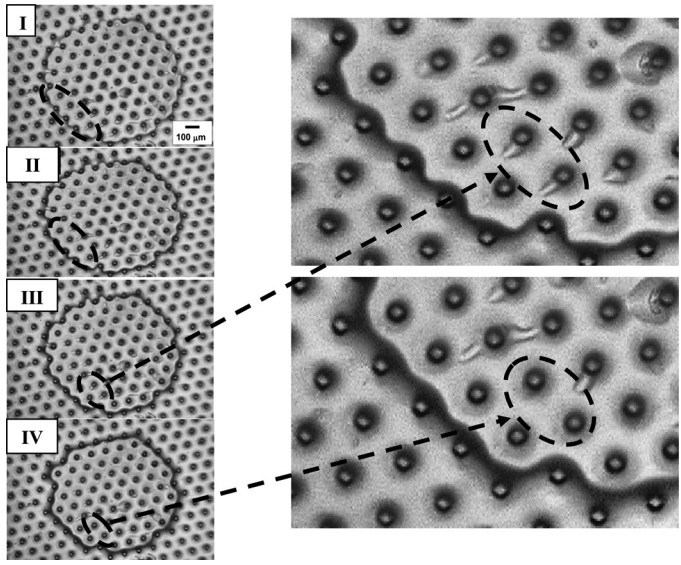

FIGURE 5 Contact micrographs during retraction of a SAM-coated glass sphere indenting a fibrillar sample with fibril height of 53 μm and nearest neighbor inter-fibrillar spacing of 87 μm at different indentation depths of (I) 20 μm, (II) 10 μm, (III) 5 μm, and (IV) −5 μm. Note the apparent disappearance of trapped pockets of water, which we propose have moved to a void nucleated under the fibril. These micrographs suggest that under these conditions void nucleation occurs at the fibrils before the crack front reaches them, which signifies a change in the controlling mode of interfacial separation. In Micrograph (I), fibrils in the dotted region have some water trapped between the contacting surfaces, while in Micrograph (II), that trapped water disappears from those fibrils before crack front reaches there. The same phenomenon at different fibrils is shown more clearly in Micrographs (III) and (IV) through magnified images.

more clearly, a magnified image corresponding to Micrograph III clearly shows the fibrils near which water is trapped and then in the magnified image corresponding to Micrograph IV the trapped water seems to have disappeared suddenly from those fibrils as the crack front approaches but before it reaches the fibril. The only conclusion we can reach is that a void nucleates at the fibril and the trapped water enters it, apparently disappearing from the cavity it originally inhabited. We find that this phenomenon occurs most significantly in the case of largest spacing and, thus, correlates with the reduction in pull-off stress, which we associate with a transition in separation mechanism from dominant interface crack growth to dominant

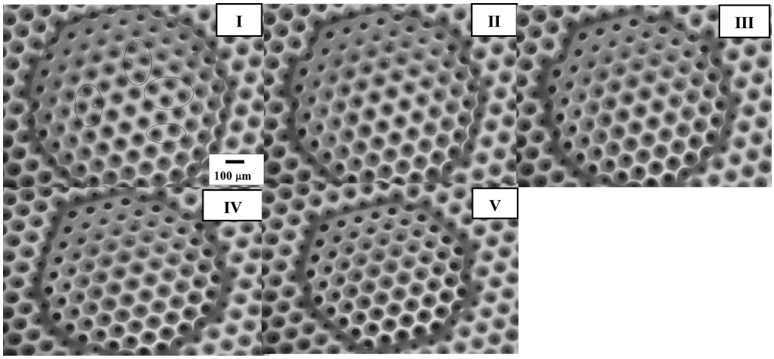

FIGURE 6 Contact micrographs during retraction of a PDMS-coated glass sphere indenting a fibrillar sample with fibril height of 53 μm and minimum inter-fibrillar spacing of 87 μm at different indentation depths of (I) 30 μm, (II) 20 μm, (III) 10 μm, (IV) 5 μm, and (V) −5 μm during retraction of the glass sphere (unloading). We observe fewer instances of trapped water pockets (for example the ones circled in I). More significantly, usually trapped water pockets do *not* disappear before crack front reaches them. Rather, they usually merge with the crack front.

interface void nucleation. Presumably, such void nucleation occurs also under dry adhesion experiments, only it is not visible. However, this phenomenon is rarely observed in the case of indentation by the PDMS-coated glass sphere as shown in micrographs in Fig. 6. This result is consistent with the higher measured pull-off force.

3.2. Effect of Roughness

Indentation tests were conducted using glass spheres with surfaces of different roughness prepared as described in Section 2.7. The maximum tensile force (pull-off force) while pulling the sphere out of contact was used as a measure of adhesion.

Force-deflection data plotted in Figs. 7(a) and 8(a) show that the pull-off force of both the flat control and fibrillar samples reduces significantly with increasing surface roughness. Figs. 7(b) and 8(b) show a series of optical micrographs of the contact region at different indentation depths. (These micrographs are for the indenter with lowest roughness.) These are very similar to those we have reported previously using a smooth, SAM-coated glass indenter [19]. In particular, they replicate the major difference between the control and fibrillar samples, *i.e.*, crack-trapping during indenter retraction in the latter case. Hence, for small roughness, the crack-trapping mechanism

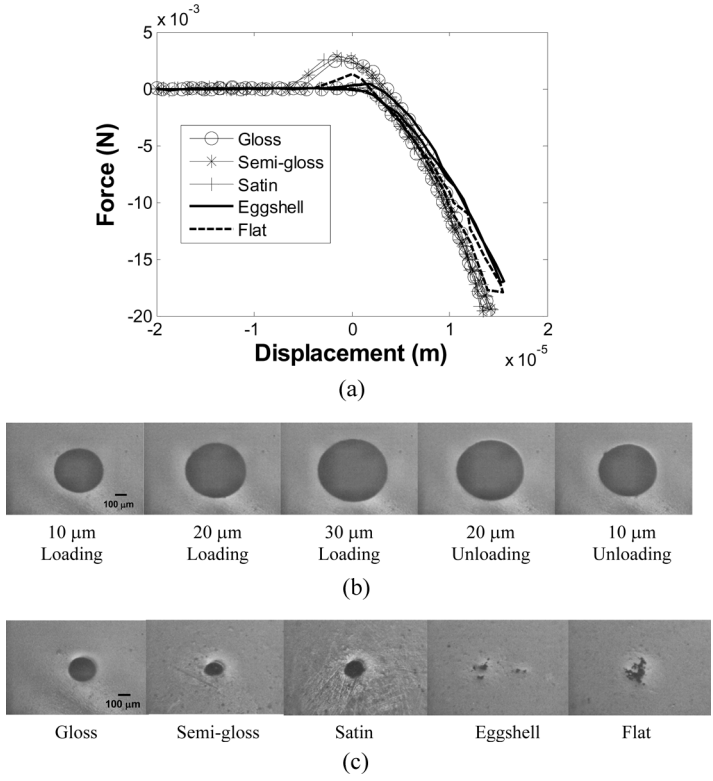

FIGURE 7 (a) Force-displacement plot obtained from normal indentation test of a flat control sample, (b) Optical micrographs of the contact area between the control sample and a painted sphere (gloss) at different indentation depths during the indentation test. The micrographs are in the order of increasing indentation depth during loading and then decreasing depths during unloading, and (c) Optical micrographs of the contact area at pull-off between the control sample and different painted spheres. The micrographs are in the order of increasing roughness of the painted sphere.

remains unaffected. Figs. 7(c) and 8(c) show the contact area when tension is maximum (the pull-off load) in the control and fibrillar samples, respectively. Again, for small roughness on both the control and fibrillar samples, the contact area appears to be similar in character to that for a flat surface. In contrast, against the rougher surfaces we observe poorly-defined and disconnected islands of contact. The fibrillar sample appears to maintain a larger overall contact perimeter, presumably because of its much higher contact compliance, but there

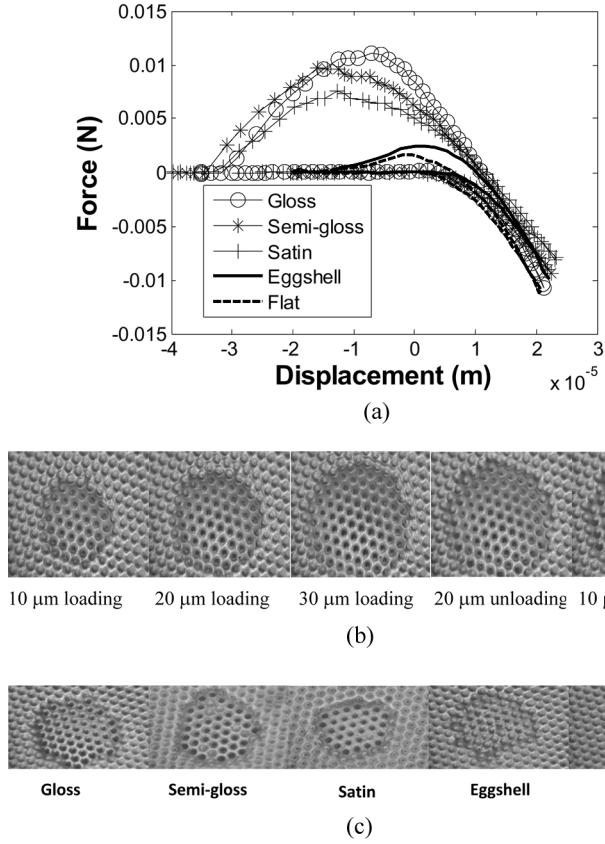

FIGURE 8 (a) Force-displacement plot obtained from normal indentation test of a fibrillar sample with fibril height of 53 μm and smallest inter-fibrillar spacing of 87 μm, (b) Optical micrographs of the contact area between the same fibrillar sample and a painted sphere (gloss, lowest roughness) at different indentation depths during the indentation test. The micrographs are in the order of increasing indentation depth during loading and then decreasing depths during unloading, and (c) Optical micrographs of the contact area at pull-off between this fibrillar sample and different painted spheres. The micrographs are in the order of increasing roughness.

is loss of contact within this perimeter for both fibrillar and flat control samples.

Figure 9(a) plots the pull-off load against different indenters in increasing order of roughness for various samples. The root mean square (RMS) roughness for different indenters is shown in Fig. 9(b). Figure 9(a) shows that fibrillar samples retain adhesion enhancement

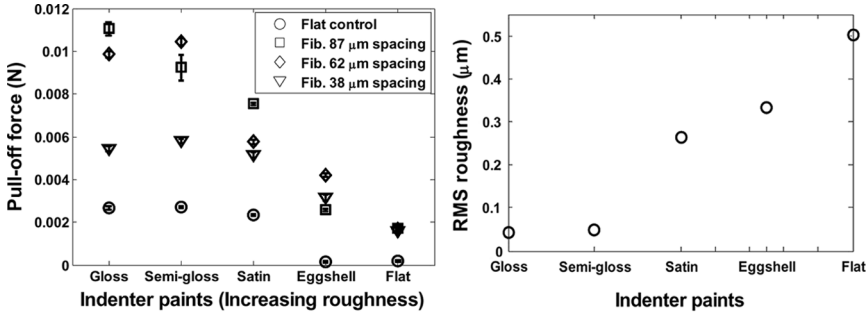

FIGURE 9 (a) Plot of pull-off force against indenter paints with increasing roughness and (b) Plot of RMS roughness of the paint surface against different paints.

over the flat control for small roughness. Pull-off force reduces for all samples with increasing roughness. Eventually, all samples have very poor adhesion. However, there is a range of intermediate roughness (*e.g.*, "eggshell") for which the control sample has essentially zero adhesion but the fibrillar samples maintain reasonably effective adhesion.

4. SUMMARY AND CONCLUSIONS

We have studied the adhesion of a film-terminated fibrillar interface under water against two hydrophobic surfaces and one hydrophilic surface, and in air against rough surfaces. Because our samples are fabricated using a hydrophobic elastomer, adhesion against hydrophobic surfaces under water is greater than in air. The adhesion measured in film-terminated samples is consistent with a multiplicative coupling of intrinsic work of adhesion with its enhancement by the crack-trapping mechanism. (We have previously shown a similar multiplicative coupling when the intrinsic work of adhesion is altered by loading rate [43].) At sufficiently large fibril spacings, a void nucleation mechanism for interfacial separation appears to dominate. Whereas for enhanced adhesion the crack-trapping mechanism favors increased separation between fibrils, the void nucleation condition favors decreased separation. Competition between these two mechanisms results in optimal inter-fibril spacing for adhesion.

Fibrillar surfaces maintain their adhesion enhancement against rough surfaces for small roughness. For sufficiently rough surfaces,

both fibrillar and flat samples show very poor adhesion. However, we find that fibrillar samples maintain considerable adhesion against eggshell and flat paints while for the flat control samples adhesion is inmeasurably small.

ACKNOWLEDGMENTS

Support from Department of Energy Grant DE-FG02-07ER46463 is acknowledged by the authors of this work. We are also grateful to the reviewers for a careful reading of the document and for their constructive comments.

REFERENCES

[1] Autumn, K., Liang, Y. A., Hsieh, S. T., Zesch, W., Chan, W. P., Kenny, T. W., and Fearing, R., *Nature* **405**, 681–684 (2000).
[2] Eisner, T. and Aneshansley, D. J., *Proc. Natl. Acad. Sci. U.S.A.* **97**, 6568–6573 (2000).
[3] Hiller, U., *Z. Morph. Tiere* **62**, 307–362 (1968).
[4] Hiller, U., *Journal of the Bombay Natural History Society* **73**, 278–282 (1975).
[5] Rizzo, N. W., Gardner, K. H., Walls, D. J., Keiper-Hrynko, N. M., Ganzke, T. S., and Hallahan, D. L., *Journal of The Royal Society Interface* **3**, 441–451 (2006).
[6] Ruibal, R. and Ernst, V., *J. Morphol.* **117**, 271–293 (1965).
[7] Scherge, M. and Gorb, S. N., *Biological Micro-And Nanotribology: Nature's Solutions*, (Springer, Berlin, 2001).
[8] Irschick, D. J., Vitt, L. J., Zani, P. A., and Losos, J. B., *Ecology* **78**, 2191–2203 (1997).
[9] del Campo, A., Greiner, C., Alvarez, I., and Arzt, E., *Adv. Mater.* **19**, 1973–1977 (2007).
[10] Glassmaker, N. J., Jagota, A., Hui, C. Y., Noderer, W. L., and Chaudhury, M. K., *Proc. Natl. Acad. Sci. U.S.A.* **104**, 10786–10791 (2007).
[11] Gorb, S., Varenberg, M., Peressadko, A., and Tuma, J., *Journal of The Royal Society Interface* **4**, 271–275 (2007).
[12] Greiner, C., Arzt, E., del Campo, A., and Foundation, V., *Adv. Mater.* **21**, 479–482 (2008).
[13] Kim, S. and Sitti, M., *Appl. Phys. Lett.* **89**, 261911-1-3 (2006).
[14] Kustandi, T. S., Samper, V. D., Ng, W. S., Chong, A. S., and Gao, H., *Journal of Micromechanics and Microengineering* **17**, 75–81 (2007).
[15] Northen, M. T. and Turner, K. L., *Nanotechnology* **16**, 1159–1166 (2005).
[16] Aksak, B., Sitti, M., Cassell, A., Li, J., Meyyappan, M., and Callen, P., *Appl. Phys. Lett.* **91**, 061906-1-3 (2007).
[17] Kim, S., Aksak, B., and Sitti, M., *Appl. Phys. Lett.* **91**, 221913-1-3 (2007).
[18] Murphy, M. P., Aksak, B., and Sitti, M., *Journal of Adhesion Science and Technology* **21**, 1281–1296 (2007).
[19] Noderer, W. L., Shen, L., Vajpayee, S., Glassmaker, N. J., Jagota, A., and Hui, C. Y., *Proc. R. Soc. London* **A 463**, 2631–2654 (2007).
[20] Schubert, B., Lee, J., Majidi, C., and Fearing, R. S., *Journal of The Royal Society Interface* **5**(25), 845–853 (2008).

[21] Shen, L., Glassmaker, N. J., Jagota, A., and Hui, C. Y., *Soft Matter* **4**, 618–625 (2008).
[22] Chaudhury, M. K. and Whitesides, G. M., *Langmuir* **7**, 1013–1025 (1991).
[23] Christenson, H. K. and Claesson, P., *Science* **239**, 390–392 (1988).
[24] Pashley, R. M., McGuiggan, P. M., Ninham, B. W., and Evans, D. F., *Science* **229**, 1088–1089 (1985).
[25] Singh, S., Houston, J., van Swol, F., and Brinker, C. J., *Nature* **442**, 526 (2006).
[26] Wood, J. and Sharma, R., *Langmuir* **11**, 4797–4802 (1995).
[27] Yushchenko, V. S., Yaminsky, V. V., and Shchukin, E. D., *J. Colloid Interface Sci.* **96**, 307–314 (1983).
[28] Lee, H., Lee, B. P., and Messersmith, P. B., *Nature (London)* **448**, 338–341 (2007).
[29] Varenberg, M. and Gorb, S., *J. R. Soc. Interface* **5**, 383–385 (2008)
[30] Fuller, K. N. G. and Tabor, D., *Proc. R. Soc. London* **A** 327–342 (1975).
[31] Johnson, K. L., Kendall, K., and Roberts, A. D., *Proc. R. Soc. London* **A**, 301–313 (1971).
[32] Briggs, G. A. D. and Briscoe, B. J., *J. Phys. D: Appl. Phys.* **10**, 2453–2466 (1977).
[33] Fuller, K. N. G. and Roberts, A. D., *J. Phys. D: Appl. Phys.* **14**, 221–239 (1981).
[34] Kim, H. C. and Russell, T. P., *J. Polym. Sci., Part B: Polym. Phys.* **39**, 1848–1854 (2001).
[35] Persson, B. N. J. and Tosatti, E., *The Journal of Chemical Physics* **115**, 5597–5610 (2001).
[36] Persson, B. N. J., *The European Physical Journal E-Soft Matter* **8**, 385–401 (2002).
[37] Guduru, P. R., *Journal of the Mechanics and Physics of Solids* **55**, 445–472 (2007).
[38] Guduru, P. R. and Bull, C., *Journal of the Mechanics and Physics of Solids* **55**, 473–488 (2007).
[39] Hui, C. Y., Glassmaker, N. J., and Jagota, A., *The Journal of Adhesion* **81**, 699–721 (2005).
[40] Bhushan, B., Peressadko, A. G., and Kim, T. W., *Journal of Adhesion Science and Technology* **20**, 1475–1491 (2006).
[41] He, B., Lee, J., and Patankar, N. A., *Colloids Surf.* **A 248**, 101–104 (2004).
[42] Long, R. and Hui, C. Y., *Proc. R. Soc. A (London)* **475**, 961–981 (2009).
[43] Vajpayee, S., Long, R., Shen, L., Jagota, A., and Hui, C. Y., *Langmuir* **25**, 2765–2771 (2009).
[44] Shen, L., Hui, C. Y., and Jagota, A., *J. Appl. Phys.* **104**, 123506-1-8 (2008).
[45] Cook, J., Gordon, J. E., Evans, C. C., and Marsh, D. M., *Proc. R. Soc. London* **A**, 508–520 (1964).
[46] Long, R., Hui, C. Y., Kim, S., and Sitti, M., *J. Appl. Phys.* **104**, 044301-1-9 (2008).
[47] Schargott, M., Popov, V. L., and Gorb, S., *J. Theor. Biol.* **243**, 48–53 (2006).
[48] Vajpayee, S., Hui, C. Y., and Jagota, A., *Langmuir* **24**, 9401–9409 (2008).
[49] Tang, T., Jagota, A., Chaudhury, M. K., and Hui, C. Y., *The Journal of Adhesion* **82**, 671–696 (2006).